

UNCLASSIFIED

Defense Technical Information Center
Compilation Part Notice

ADP012501

TITLE: Experimental Dynamics of Stressed, Strongly Correlated
Magnetized Plasmas

DISTRIBUTION: Approved for public release, distribution unlimited

This paper is part of the following report:

TITLE: Non-Neutral Plasma Physics 4. Workshop on Non-Neutral Plasmas
[2001] Held in San Diego, California on 30 July-2 August 2001

To order the complete compilation report, use: ADA404831

The component part is provided here to allow users access to individually authored sections of proceedings, annals, symposia, etc. However, the component should be considered within the context of the overall compilation report and not as a stand-alone technical report.

The following component part numbers comprise the compilation report:

ADP012489 thru ADP012577

UNCLASSIFIED

Experimental Dynamics of Stressed, Strongly Correlated Magnetized Plasmas

T. B. Mitchell*, J. J. Bollinger[†], W. M. Itano[†] and D. H. E. Dubin**

*Department of Physics and Astronomy, University of Delaware, Newark, DE 19716

[†]Time and Frequency Division, National Institute of Standards and Technology, Boulder, CO 80305

**Department of Physics, University of California at San Diego, La Jolla, CA 92093

Abstract. We study the control of the rotation of a laser-cooled ion crystal in a Penning trap by a rotating electric field perturbation. We show that application of a small torque produces sudden angular jumps or ‘slips’ of the crystal orientation spaced by intervals when the crystal is phase-locked or ‘stuck’ relative to the rotating perturbation. The distribution of angular slips is described by a power law, where the power-law exponent depends on the applied torque. We believe this system is driven by a constant force and that small perturbations or thermal effects trigger the slips.

Non-neutral plasmas confined in Penning-Malmberg traps are used in a variety of experiments including plasma physics, Coulomb crystal studies, precision spectroscopy, antimatter research, and storage of highly charged ions [1]. Recently there has been a great deal of interest in using a rotating electric field perturbation to control the global $\mathbf{E} \times \mathbf{B}$ rotation of these plasmas [2, 3, 4]. For crystallized ion plasmas, phased-locked control of the plasma rotation has been demonstrated [4], which has important implications for atomic clocks [5] and for quantum computation with trapped ions [6].

In this manuscript we study the limits to phase-locked control due to the application of a small torque produced by the radiation pressure of a weak laser beam. We observe sudden angular jumps or ‘slips’ of the crystal orientation spaced by intervals when the crystal orientation is phase-locked or ‘stuck’ relative to the rotating perturbation. Stick-slip behavior similar to that observed here is found in many different and diverse systems: for example, in studies of friction between two surfaces [7, 8], in experiments on avalanches and slips in granular systems [9, 10, 11], and as the underlying process in spring-block models of earthquakes [12, 13]. Many of these systems, including the study presented here, exhibit a power-law distribution of the slip amplitudes, indicative of an underlying critical point [14, 15].

Our work uses the Penning-Malmberg trap at NIST to store $\sim 20,000$ $^9\text{Be}^+$ ions. The ions interact by unscreened Coulomb repulsion and are Doppler laser-cooled [16] to millikelvin temperatures, where they become strongly coupled. The degree of coupling is quantified by the Coulomb coupling parameter,

$$\Gamma \equiv \frac{1}{4\pi\epsilon_0} \frac{e^2}{a_{\text{ws}} k_B T}, \quad (1)$$

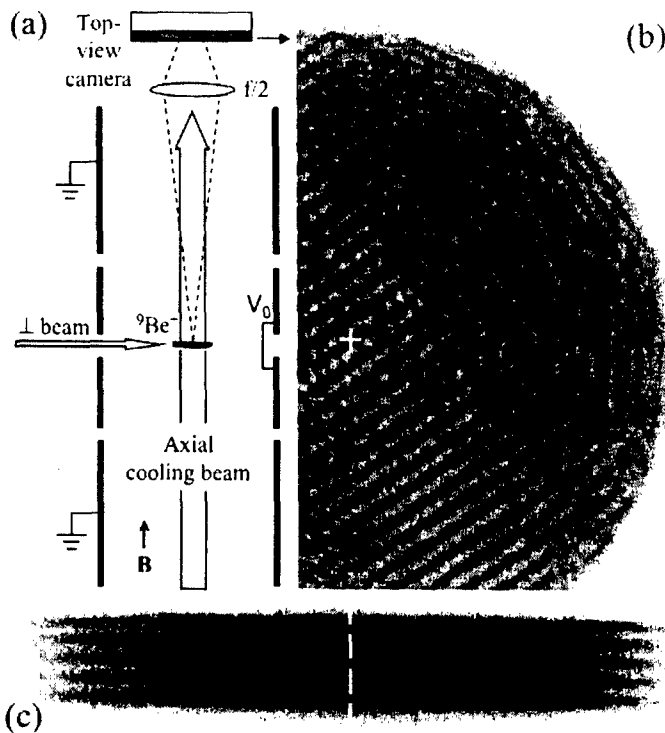


FIGURE 1. (a) Schematic of the cylindrical Penning trap and the top-view imaging system. The side-view imaging system is not shown. (b) Strobed top-view image of a 5 axial plane ${}^9\text{Be}^+$ ion crystal with a bcc structure, similar to those used in this study. (c) Side-view image (unstrobed) of the same ion crystal. The diameter ($2r_{Bc}$) of the ${}^9\text{Be}^+$ ions is $495\ \mu\text{m}$. Ions of greater mass are located at $r > r_{Bc}$, but do not fluoresce in the laser beam. The rotation axes are indicated.

which is the ratio of the Coulomb potential energy of neighboring ions to the kinetic energy per ion. Here, ϵ_0 is the permittivity of the vacuum, e is the charge of an ion, k_B is Boltzmann's constant, T is the temperature, and a_{ws} is the Wigner-Seitz radius, defined by $4\pi(a_{ws})^3/3 = 1/n_0$, where n_0 is the ion number density. With coupling parameters greater than $\Gamma \simeq 1$ the ions are strongly coupled [17], and when $\Gamma \geq 172$ they form a Coulomb crystal (a classical Wigner crystal) [18, 19]. Structurally similar Coulomb crystals are believed to exist in dense astrophysical matter, such as the interior of white dwarfs and the outer crust of neutron stars [20]. Interestingly, observations of power-law statistics of soft γ -ray (SGR) events have recently been interpreted as evidence that the Coulomb crystal comprising the outer crust of a magnetized neutron star can undergo very large-scale slips ('starquakes') [21, 22]. The measured power law exponents of the neutron starquakes lie within the range of exponents we measure here (see Fig. 3).

Figure 1(a) shows the experimental setup [4, 19]. We create ${}^9\text{Be}^+$ ions by ionizing ${}^9\text{Be}$ atoms in a separate trap (not shown) and then transferring the ions to the main trap for experimentation [23]. The ${}^9\text{Be}^+$ ions were confined radially by a uniform magnetic

field $B=4.465$ T (cyclotron frequency $\Omega_c/2\pi = 7.608$ MHz) in the \hat{z} direction and axially by a potential difference of $V_0 = -500$ V applied between the center and end electrodes of the trap. Near the trap center the trap potential is quadratic and given by $m\omega_z^2(z^2 - r^2/2)/(2e)$, where the axial frequency $\omega_z/2\pi = 565$ kHz for ${}^9\text{Be}^+$. Here r and z denote the cylindrical radius and axial coordinates. Due to the axial magnetic field and the radial components of the ion space charge and trap electric fields, the ion crystal rotates at a frequency ω_r about the trap symmetry axis \hat{z} .

In our work the plasma has had sufficient time to evolve to a thermal equilibrium state where its rotation and density is uniform across the cloud [24]. For 20,000 trapped ions with $\omega_r/2\pi = 22.8$ kHz (typical of this work), the ion plasma has a density of 7.1×10^7 cm^{-3} and a lenticular shape with a radial diameter $2r_0 \approx 1$ mm and an aspect ratio $\alpha = z_0/r_0 \approx 0.05$. Here, $2z_0$ denotes the axial extent of the plasma at $r = 0$. In addition to ${}^9\text{Be}^+$ ions, ions of greater mass ('heavy ions') such as BeH^+ and BeOH^+ are created by reactions with ${}^9\text{Be}^+$ ions and background neutral molecules. For the work discussed here, typically 20 % to 50 % of the plasma consisted of heavy impurity ions. These ions are sympathetically cooled to temperatures similar to the ${}^9\text{Be}^+$ ions and, due to the rotation, centrifugally separate to larger radii, where they crystallize [25, 26].

To control ω_r , we applied an electric field perturbation rotating about the \hat{z} axis at frequency ω_{rp} [4]. The rotating perturbation applies a torque on the radial boundary of the plasma (on the non-fluorescing, heavy ions) by creating a small-amplitude traveling wave. The torque due to this wave is then transferred to the plasma interior through the strong inter-particle Coulomb forces, which act to bring the plasma to the same rotation frequency as ω_{rp} [24]. We observe similar stick-slip motion with both dipole and quadrupole rotating fields. However, most measurements, including those we report here, were taken with a dipole rotating field.

The radial binding force of the trap is due to the Lorentz force produced by the plasma's rotation through the magnetic field. Therefore changing ω_r changes the radial binding force of the trap and provides a sensitive way to adjust the overall shape and structural phase of the plasma. In this work, the frequency of the rotating perturbation ω_{rp} was kept near $2\pi \times 22.8$ kHz and slightly adjusted to produce a disk-shaped plasma consisting of 5 axial planes with a bcc-like crystal structure in the plasma center [19]. Because $\omega_r \ll \Omega_c$, the ion motion in a direction perpendicular to the magnetic field is determined principally by $\mathbf{E} \times \mathbf{B}$ guiding center dynamics [27].

The main cooling-laser beam ($\lambda = 313$ nm) was directed along the z axis and tuned 10 to 20 MHz lower in frequency than a hyperfine-Zeeman component of the $2s\ ^2S_{1/2} \rightarrow 2p\ ^2P_{3/2}$ resonance with a natural linewidth of 19 MHz. This beam's power was ~ 50 μW and the beam was focused to a ~ 0.5 mm waist at the ion crystal. A second cooling beam (\perp beam in Fig. 1(a)), derived from the same laser, was directed perpendicularly to \hat{z} and had a ~ 70 μm waist and ~ 1 μW power. Both the perpendicular and parallel cooling lasers were required to form a well defined crystal in the disk-shaped plasmas discussed here. Although we did not measure the ion temperature, the theoretical cooling limit is 0.5 mK, and an experimental upper bound of $T < 10$ mK has been measured in previous experiments [23]; for a density of $n_0 = 7.1 \times 10^7$ cm^{-3} , these limits give a range of $112 < \Gamma < 2230$. An indirect estimate of the ions' coupling parameter, based on observations of when the bcc(110) structural phase was exclusively favored, is $\Gamma \sim 600$

[28].

The \perp beam is normally directed through the radial center ($r = 0$) of the crystal in order to minimize its applied torque while providing a low Doppler-cooling temperature [16]. In this experiment, we offset the \perp -beam position slightly (5 to 30 μm) from the plasma center to produce a torque on the $^9\text{Be}^+$ ions in the same direction as the plasma rotation. The resultant torque from the \perp beam was larger than any other ambient torque due to, for example, resonances between modes and asymmetries in the trap construction [29] or background gas drag [30].

A series of lenses formed side- and top-view images of the ion fluorescence, with viewing directions perpendicular and parallel to the magnetic field respectively, on either a gateable charge-coupled device (CCD) camera, or on an imaging photomultiplier tube. The resolution of the optical systems was $\sim 4 \mu\text{m}$, while typical interparticle spacings were $\sim 15 \mu\text{m}$. By detecting the ion fluorescence synchronously with the rotating perturbation drive, images of the individual ions that make up the Coulomb crystals were obtained. Figure 1(b) shows a strobed, top-view CCD camera image of a 5-axial plane crystal in the bcc structural phase, accumulated over 40 s. The ion positions are well localized in the plasma center; however, at larger radii they are blurred.

To investigate the blurring we used an imaging photomultiplier tube in the top-view position to record the positions and detection times of the fluorescence photons. Data sets consisted of 125 ms intervals of data recorded each second over long periods of time (up to 5000 s). Images similar to those in Fig. 1(b) were created for each 125 ms interval by constructing 2D histograms of the ion fluorescence in the frame of the rotating perturbation. The orientation θ_{cry} of the central crystallized region in the rotating frame was determined (modulo π due to the bcc crystal bilateral symmetry) with an uncertainty of $\sim 0.002\pi$ radians [31].

In Fig. 2 we plot $\theta_{\text{cry}}(t)$ for two data sets that differ mainly in the amount of \perp -beam torque. Over long time scales the \perp -beam torque produces a slightly faster rotation (a rotational ‘creep’) of the $^9\text{Be}^+$ crystal relative to the rotating perturbation. For example, in data set 2 $\Delta\omega \equiv \omega_r - \omega_p \approx 2\pi \times 8 \text{ mHz}$. Over shorter time scales, as shown in the inset of Fig. 2, much of this crystal rotation takes place with sudden jumps in θ_{cry} , ‘slips’, whose time scale is too fast to be captured by the top-view diagnostic. Intermittent behavior is a common feature in the plastic deformation (creep) of many materials (see [32] for references). Let $\Delta\theta_{\text{cry}}$ denote the angular displacement between two successive measurements of θ_{cry} . The statistics of $\Delta\theta_{\text{cry}}$ consists of a normal distribution (from measurement error) centered about zero with a width of $\sim 0.002\pi$, and infrequent larger slips. Due to the known sign of the \perp -beam torque and the π ambiguity mentioned above, we choose $\Delta\theta_{\text{cry}}$ to lie in the range $[0, \pi)$. To separate statistically significant slips from measurement error we further require $0.007\pi \leq \Delta\theta_{\text{cry}} \leq 0.97\pi$. We find that statistically significant slips account for greater than 90 % of the measured change in θ_{cry} .

The \perp -beam torque is applied to all the $^9\text{Be}^+$ ions in the radial interior of the crystal. The rotating perturbation, however, applies its torque on the outer radial boundary of the heavy ions. We therefore believe the stress due to the competition between these torques is greatest in the region of the heavy ions and anticipate that the slips of Fig. 2 are due to ion motion between the radial boundary of the $^9\text{Be}^+$ ions, r_{Be} , and the overall radial boundary of the plasma, r_0 . This is supported by the top-view images and by simulation

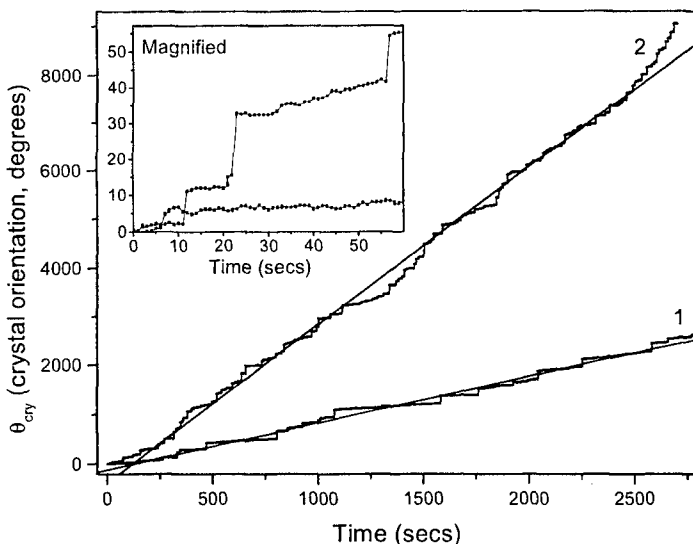


FIGURE 2. Crystal orientation θ_{cry} in the frame of the rotating perturbation for two data sets with different \perp -beam torques. The torque is greater in data set 2. The lines are from a linear regression fit. The inset shows a magnified plot of the first 60 s of data.

work discussed below, which show most slips occurring as approximate rigid rotations of the ${}^9\text{Be}^+$ ions. Because the simulation slips occur at a radius slightly greater than r_{Be} , and r_{Be} varied from data set to data set, we characterize a slip amplitude A_{slip} by the linear distance $\Delta\theta_{cry}r_{Be}$.

Figure 3 shows the distribution $f(A_{slip})$ of slips for the two data sets shown in Fig. 2. Because we can not distinguish between slips with amplitude A_{slip} or $A_{slip} + n\pi r_{Be}$, where n is an integer, we fitted to the function $f_{slip} \propto \sum_{n=0}^{n_{cut}} (A_{slip} + n\pi r_{Be})^{-\gamma}$ to determine the agreement of the data with a power law distribution. Here n_{cut} is a cutoff that could depend on the system size, creep rate, or other factors. We obtain a good fit for any n_{cut} but find that χ^2 goes through a weak minimum at $n_{cut}=6$, and therefore use that value in the following analysis. This results in measured γ s slightly larger ($<10\%$ and within the uncertainty of the fit) than those resulting from $n_{cut}=1$. In the insert of Fig. 3 we plot the measured power-law exponent γ as a function of the creep rate $\Delta\omega \cdot r_{Be}$ for 10 data sets with the same rotating perturbation strength but different \perp -beam torques. We find that γ decreases as the creep rate, a measure of the applied \perp -beam torque, increases. Decreases in the stick-slip exponent with increased drive have been observed in some experimental systems [8, 33, 34], but not in all [32].

Inspection of Fig. 2 shows that the waiting periods (the time intervals between successive slips) are typically many seconds. An analysis of the waiting periods shows a peaked distribution with median waiting periods ranging from 4 s for the highest \perp -beam torques to 12 s for the lowest \perp -beam torques. In Fig. 4 we plot the frequency of slips versus waiting time for a data set with moderate torque. The frequency was normalized as before by dividing the number of slips n_{slip} by the binwidth and the duration

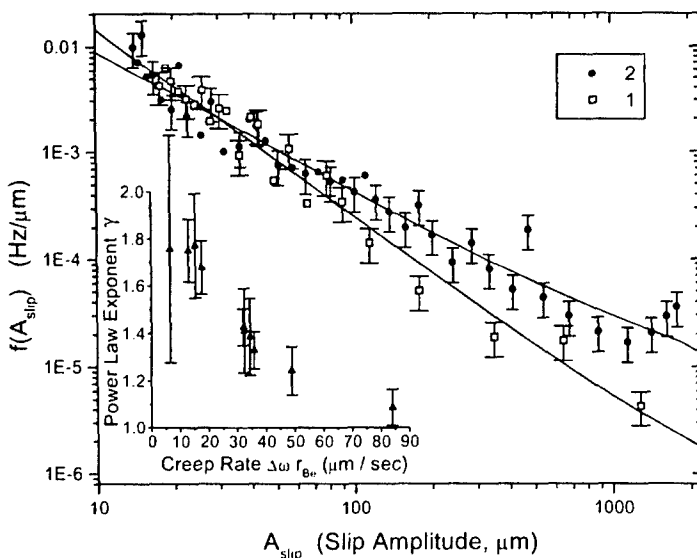


FIGURE 3. Distribution $f(A_{slip})$, where $f(A_{slip})dA_{slip}$ is the frequency of slips between A_{slip} and $A_{slip} + dA_{slip}$, for the two data sets shown in Fig. 2. The lines are fits to a power law with a cutoff as described in the text. The insert shows the measured power-law exponent γ versus applied torque, as parameterized by the creep rate, for all of the data sets.

of the data set (4882 s).

Earthquakes are another phenomena that exhibit power-law frequency versus amplitude behavior and peaked waiting time distributions. Although there has been no consensus on which is the 'correct' distribution, it has been suggested that the waiting-time distributions of earthquakes can be described by lognormal [35], Weibull [36] or Gaussian [37] statistics. In Fig. 4 we also plot 3-parameter fits of the data to these distributions. The Weibull distribution, often used to model the time until failure of brittle materials, is

$$\rho(t) = A_0 \frac{m t^{m-1} e^{-(t/t_0)^m}}{t_0^m}, \quad 0 < t < \infty, \quad m > 0, \quad (2)$$

and has a median waiting time value of $t_{med} = (\log 2)^{1/m} t_0$. A Weibull model for failure can be derived theoretically as a form of an extreme-value distribution, governing the time to failure of the 'weakest link' of many competing processes [38]. When the shape parameter $m = 1$, the Weibull distribution reduces to the exponential distribution $\rho(t) = A_0 e^{-(t/t_0)}$. The exponential distribution is produced by a system with a constant failure rate and thus no dependence on the state of the system (i.e., it is 'memoryless'). Distributions where $m \neq 1$ result when the outcome of a trial depends in part on how long the trial has been conducted.

As seen in Fig. 4, the fit to a Weibull distribution results in a significantly smaller χ^2 (chi squared per degree of freedom), and this is true for the other data sets as well. If we sum up the χ^2 of fits for all of the 10 data sets, the Gaussian and lognormal

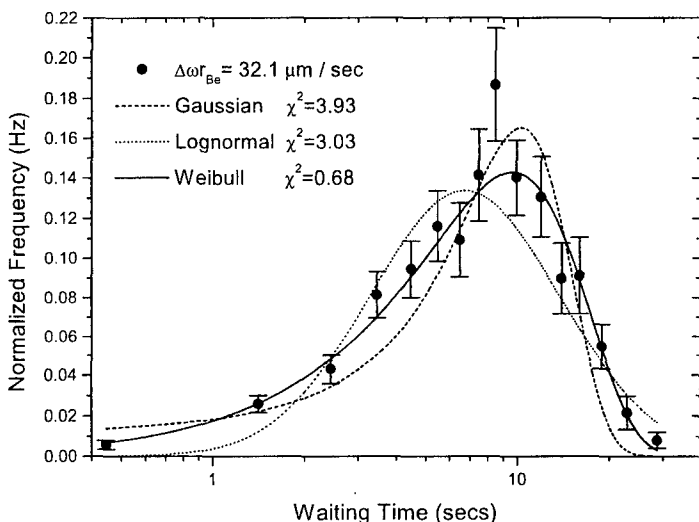


FIGURE 4. Distribution of waiting times between slips for a data set with a moderate torque.

fits have statistically the same value (18.5 and 21.1), but the Weibull fit produces $\Sigma \chi^2 = 10.8$. The average and standard deviation of the shape parameter m is 1.96 ± 0.35 , perhaps indicating that the ion crystal has a ‘memory.’ For large m , $p(t)$ approaches a delta function. Ward and Goes [36] have used $v = 1/m$ to parameterize the degree of aperiodicity, and found in their earthquake simulation data that as they increased the magnitudes of the quakes considered, both t_{med} and m increases. We also find these trends in our ion-crystal data.

Previous workers in the analysis of SGR ‘starquake’ statistics have looked for correlations between waiting times and the amplitude of the γ -ray burst. In order to investigate this with our data, we sorted a total of 918 slips from 4 data sets with similar torque by increasing slip amplitude, and then into groups of ~ 150 slips. We next fitted the time intervals of each of these groups to a Weibull distribution. We did this both for the time interval until the next slip of any amplitude (Δt^+) and for the interval from the previous slip (Δt^-). The results are plotted in Fig. 5, and show evidence for increasing t_{med} for Δt^- , and much less or no correlation for Δt^+ . This is at variance with results from SGRs, where either no correlation has been seen [21, 39, 40], or an anticorrelation seen for Δt^+ [41].

Most experiments exhibiting stick-slip behavior are performed with ‘constant-velocity driving’ where the force is applied through an effective elastic coupling [8, 9, 10]. The driving force of the system is something like $F(t) = K(Vt - x(t))$ where ‘ x ’ is the ‘position’ of an element in the system (for example, the position of a bead or slider block in a chain), K is the effective spring constant that couples the applied force to each element in the system, and V is the constant average velocity that is imposed on the system. Stick-slip motion occurs for small V and K , and a critical point exists in the limit $V \rightarrow 0$ and $K \rightarrow 0$ [15, 33]. If the system gets stuck, it will eventually slip again

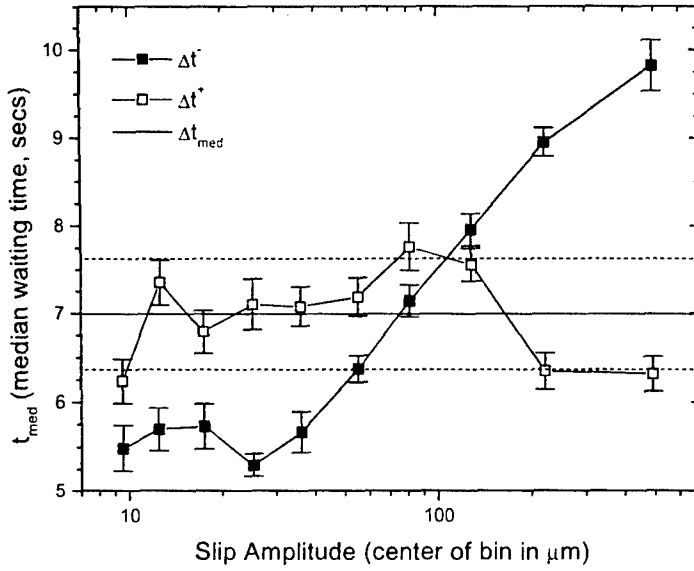


FIGURE 5. Measured t_{med} versus slip amplitude. The lines indicate the mean value and standard deviation measured for random slip amplitudes.

because the driving force increases linearly until slip occurs.

However, our experiment is performed under conditions more similar to ‘constant-force driving’ since the \perp -beam radiation-pressure force is constant in time and applied directly to the ${}^9\text{Be}^+$ ions. In constant-force driving the system undergoes a depinning transition at a critical force F_c and moves with constant average velocity proportional to $(F - F_c)^\beta$ for $F > F_c$ and critical exponent β [33]. If a constant-force system gets stuck for a long period of time, then this indicates $F < F_c$ and the system should permanently stick.

In fact the observed waiting times (Fig. 4) are long compared to any known dynamical time scales due to internal modes of the system. Why doesn’t the system permanently stick? One possibility is that the slips could be excited by an external perturbation. By deliberately modulating the amplitude of the cooling and torquing lasers we have established that the amplitude noise present in these beams is not high enough to trigger slips. Another source of perturbations is the neutral atoms of the $\sim 10^{-8}$ Pa vacuum background. We have measured that the relative abundance of ${}^9\text{Be}^+$ ions to heavy impurity ions decreases with an e-folding time of ~ 10 hours, due to collisions with background neutrals. With a cloud of 20,000 ions, this gives a median time between collisions of ~ 1.25 s. However, the relationship between these collisions and slips, if any, is unclear. For example, if all slips were caused simply by collisions, the waiting time distribution for slips would be exponential, in contrast to what is observed.

We have performed molecular-dynamics simulations with 1000 ions (40 % ${}^9\text{Be}^+$, 60 % heavy ions) with the goal of better understanding the dynamics and origin of the slips. About four months of computation time has been required to simulate the

equivalent of ~ 1.2 s of experimental time. The simulations have produced three events which can be interpreted as slips. In these events, a rearrangement of a small number of heavy ions in the vicinity of a lattice defect produces a sudden change in the orientation of the crystal. Once started, the slip eventually stops because the driving force of the \perp -beam is not sufficient to sustain continuous motion. Because it appears that the rearrangement of a few ions can trigger a slip, thermal fluctuations of the ions may be responsible for starting the slips in both experiment and simulation. However, the simulations also show the presence of a torsion mode of large amplitude and low frequency (~ 10 Hz) that produces a time-dependent stress which may also play a role in triggering slips. This mode was not observed in the experimental data, possibly because of damping from laser cooling.

In summary, we have observed creep and stick-slip motion in the rotational control of laser-cooled ion crystals in a Penning trap. We believe this system is constant-force driven and may be an experimental example of a subcritical state [15] where the slips are triggered by thermal fluctuations or by other as yet unidentified perturbations such as collisions with neutral background atoms. The trapped-ion crystal system discussed here possesses most of the features of a self-organized critical state [14, 15]. Therefore further investigations of the stick-slip behavior over a wider range of control parameters (\perp -beam torque, temperature, rotating perturbation strength, background pressure) could be useful for understanding the applicability of this concept to real physical systems. Finally, minimizing the occurrence of the slips is important for some applications [5, 6]. This can be done by minimizing the \perp -beam torque, either through active control of the \perp -beam position or by appropriate tailoring of the \perp -beam profile [42]. Increasing the strength of the rotating electric field perturbation should also decrease the frequency of slips due to small ion rearrangements. Two data sets taken with half the rotating perturbation strength of the data sets analyzed here showed an increase in the number of slips and rotational creep of the ion crystal.

ACKNOWLEDGMENTS

This research was supported by the Office of Naval Research and the National Science Foundation (Dubin). We thank S. Zapperi, R. L. Kautz, J. M. Kriesel, J. P. Schiffer, and D. J. Wineland for useful comments, and B. M. Jelenković and X.-P. Huang for technical assistance.

REFERENCES

1. Anderegg, F., Schweikhard, L., and Driscoll, C. F., editors, *Non-Neutral Plasma Physics IV*, AIP, New York, 2001.
2. Greaves, R. G., and Surko, C. M., *Phys. Rev. Lett.*, **85**, 1883–1886 (2000).
3. Hollmann, E. M., Anderegg, F., and Driscoll, C. F., *Phys. Plasmas*, **7**, 2776–2789 (2000).
4. Huang, X.-P., Bollinger, J. J., Mitchell, T. B., and Itano, W. M., *Phys. Plasmas*, **5**, 1656–1663 (1998).
5. Tan, J. N., Bollinger, J. J., and Wineland, D. J., *IEEE Trans. Instrum. Meas.*, **44**, 144–147 (1995).
6. Cirac, J. I., and Zoller, P., *Phys. Rev. Lett.*, **74**, 4091–4094 (1995).
7. Demirel, A. L., and Granick, S., *Phys. Rev. Lett.*, **77**, 4330–4333 (1996).

8. Ciliberto, S., and Laroche, C., *J. Phys. I France*, **4**, 223–235 (1994).
9. Nasuno, S., Kudrolli, A., and Gollub, J. P., *Phys. Rev. Lett.*, **79**, 949–952 (1997).
10. Albert, I., Tegzes, P., Kahnig, B., Albert, R., Sample, J. G., Pfeifer, M., Barabási, A.-L., Vicsek, T., and Schiffer, P., *Phys. Rev. Lett.*, **84**, 5122–5125 (2000).
11. Frette, V., Christensen, K., Malthe-Sørenssen, A., Feder, J., Jøssang, T., and Meakin, P., *Nature*, **379**, 49–52 (1996).
12. Olami, Z., Feder, H. J. S., and Christensen, K., *Phys. Rev. Lett.*, **68**, 1244–1247 (1992).
13. Burridge, R., and Knopoff, L., *Bull. Seismol. Soc. Am.*, **57**, 341–371 (1967).
14. Bak, P., Tang, C., and Wiesenfeld, K., *Phys. Rev. Lett.*, **59**, 381–384 (1987).
15. Vespignani, A., and Zapperi, S., *Phys. Rev. E*, **57**, 6345–6362 (1998).
16. Itano, W. M., Brewer, L. R., Larson, D. J., and Wineland, D. J., *Phys. Rev. A*, **38**, 5698–5706 (1988).
17. Ichimaru, S., Iyetomi, H., and Tanaka, S., *Phys. Rep.*, **149**, 91–205 (1987).
18. Itano, W. M., Bollinger, J. J., Tan, J. N., Jelenković, B., Huang, X.-P., and Wineland, D. J., *Science*, **279**, 686–689 (1998).
19. Mitchell, T. B., Bollinger, J. J., Dubin, D. H. E., Huang, X.-P., Itano, W. M., and Baughman, R. H., *Science*, **282**, 1290–1293 (1998).
20. Van Horn, H. M., *Science*, **252**, 384–389 (1991).
21. Cheng, B., Epstein, R. I., Guyer, R. A., and Young, A. C., *Nature*, **382**, 518–520 (1996).
22. Göğüş, E., Woods, P. M., Kouveliotou, C., van Paradijs, J., Briggs, M. S., Duncan, R. C., and Thompson, C., *Astrophys. J.*, **532**, L121–L124 (2000).
23. Brewer, L. R., Prestage, J. D., Bollinger, J. J., Itano, W. M., Larson, D. J., and Wineland, D. J., *Phys. Rev. A*, **38**, 859–873 (1988).
24. Dubin, D. H. E., and O'Neil, T. M., *Rev. Mod. Phys.*, **71**, 87–172 (1999).
25. O'Neil, T. M., *Phys. Fluids*, **24**, 1447–1451 (1981).
26. Larson, D. J., Berquist, J. C., Bollinger, J. J., Itano, W. M., and Wineland, D. J., *Phys. Rev. Lett.*, **57**, 70–73 (1986).
27. Dubin, D. H. E., and O'Neil, T. M., *Phys. Rev. Lett.*, **60**, 511–514 (1988).
28. Mitchell, T. B., Bollinger, J. J., Huang, X.-P., Itano, W. M., and Dubin, D. H. E., *Phys. Plasmas*, **6**, 1751–1758 (1999).
29. Mitchell, T. B., Bollinger, J. J., Huang, X.-P., and Itano, W. M., "Crystalline Order in Strongly Coupled Plasmas", in *Trapped Charged Particles and Fundamental Physics*, edited by D. H. E. Dubin and D. Schneider, AIP, New York, 1999, pp. 309–318.
30. Wineland, D. J., Bollinger, J. J., Itano, W. M., and Prestage, J. D., *J. Opt. Soc. Am. B*, **2**, 1721–1729 (1985).
31. The crystal images occasionally showed defect lines that moved slowly across the crystal and prevented a definitive measurement of θ_{cry} . This occurred more frequently with larger torque. In this case shorter time series separated by intervals when θ_{cry} could not be unambiguously determined were appended to each other without introducing discontinuities in θ_{cry} at the junctures.
32. Miguel, M.-C., Vespignani, A., Zapperi, S., Weiss, J., and Grasso, J.-R., *Nature*, **410**, 667–671 (2001).
33. Lacombe, F., Zapperi, S., and Hermann, H. J., *Phys. Rev. B*, **63**, 104104 (2001).
34. Zapperi, S., Cizeau, P., Durin, G., and Stanley, H. E., *Phys. Rev. B*, **58**, 6353–6366 (1998).
35. Nishenko, S. P., and Buland, R., *Bull. Seismol. Soc. Am.*, **77**, 1382 (1987).
36. Ward, S. N., and Goes, S. D. B., *Geophys. Res. Lett.*, **20**, 2131–2134 (1993).
37. Pepke, S. L., Carlson, J. M., and Shaw, B. E., *J. Geophys. Res.*, **99**, 6769–6788 (1994).
38. Weibull, W., *J. Appl. Mech.*, **9**, 293–297 (1951).
39. Laros, J. G., Fcnimore, E. E., Klebesadel, R. W., Atteia, J.-L., Boer, M., Hurley, K., Neil, M., Vedrenne, G., Kane, S. R., Kouveliotou, C., Cline, T. L., Dennis, B. R., Desai, U. D., Orwig, L. E., Kuznetsov, A. V., Sunyaev, R. A., and Terekhov, O. V., *Astrophys. J.*, **320**, L111–L115 (1987).
40. Vidale, J. E., Ellsworth, W. L., Cole, A., and Marone, C., *Nature*, **368**, 624–626 (1994).
41. Göğüş, E., Woods, P. M., Kouveliotou, C., van Paradijs, J., Briggs, M. S., Duncan, R. C., and Thompson, C., *Astrophys. J.*, **526**, L93–L96 (1999).
42. The \perp -beam torque can be reduced with a beam that has a large waist and frequency dispersion across the waist that matches the ion Doppler shifts due to the plasma rotation.